Table S1. Crystallographic Summary of Glo qRRMs, Related to Figure 1.

	Glo qRRM1	Glo qRRM2	Glo qRRM3
Data Collection			
Space group	C2	$P2_1$	$P4_22_12$
Cell Dimensions			
a, b, c (Å)	115.2, 27.7, 66.4	45.7, 29.0, 69.5	55.5, 55.5, 58.7
α, β, γ (°)	90.0, 109.4, 90.0	90.0, 106.8, 90.0	90.0, 90.0, 90.0
Resolution (Å)	50.0-1.54 (1.60-1.54)*	50.0-1.55 (1.58–1.55)*	50.0-1.99 (2.06-1.99)*
Rmerge (%)	6.5 (11.5)*	5.0 (25.7)*	6.2 (22.5)*
I/σI	20.2 (6.0)*	34.6 (4.0)*	32.4 (9.9)*
Completeness (%)	90.9 (70.3)*	93.4 (70.7)*	95.9 (86.4)*
Redundancy	3.3 (1.4)*	3.4 (2.4)*	12.5 (11.0)*
Refinement			
Resolution (Å)	22.4–1.54	32.5–1.55	24.8–1.99
No. reflections	26,927	23,923	6,311
R_{work} /R_{free} (%)	17.4/20.8	19.3/23.9	22.0/26.0
No. of Atoms			
Protein	1,380	1,495	685
Ligand/Ion	40	0	23
Water	230	127	33
B-Factors			
Protein	17.5	25.3	28.1
Ligand/Ion	37.4	–	48.5
Water	29.1	32.0	31.6
RMS Deviations			
Bond lengths (Å)	0.009	0.011	0.010
Bond angles (°)	1.04	1.07	1.23
Ramachandran plot (%)			
Favored	99.4	97.8	98.7
Allowed	0.6	2.2	1.3
PDB ID	5UZG	5UZM	5UZN

Table S2. Identification of Glo residues critical for G-tract or TCEIII recognition, Related to Figure 4.

Glo qRRM1,2	RNA motif recognized	Mutated domain	$TCE_{GAG/UUC}$ K_d (μM)[1]	K_{rel}	p-value[2]	AGGGA K_d (μM)[1]	K_{rel}	p-value[2]
WT	G-tract, TCEIII	NA	8.9 ± 0.6	1.0		0.28 ± 0.009	1.0	
W58A	G-tract	qRRM1	15.9 ± 0.3	1.8	0.0006	0.54 ± 0.04	1.9	0.007
Y155A	G-tract	qRRM2	14.5 ± 0.5	1.6	0.003	0.25 ± 0.02	0.9	0.996
W58A,Y155A	G-tract	qRRM1&2	22.3 ± 0.6	2.5	0.0001	>60	>200	0.024
R52A	TCEIII	qRRM1	19.4 ± 0.5	2.2	0.0001	0.59 ± 0.03	2.1	0.002
K149A	TCEIII	qRRM2	29.7 ± 1.9	3.3	0.0001	0.22 ± 0.003	0.8	0.846
R52A,K149A	TCEIII	qRRM1&2	>60	>7	0.008	0.93 ± 0.10	3.3	0.0001

[1]K_d values for binding of wild-type (WT) and mutant qRRM1,2 proteins to either $TCE_{GAG/UUC}$, 5′-AGGGA, or TCEI RNAs are shown as mean ± SEM from three technical replicates.

[2]P-values were calculated for mutant binding to the $TCE_{GAG/UUC}$ or 5′-AGGGA RNA relative to the WT protein using a one-way ANOVA, excluding the double mutants whose binding was too weak to determine precisely and are reported as a lower limit of >60 μM. The p-values for qRRM1,2^{R52A,K149A} mutant binding to $TCE_{GAG/UUC}$ or TCEI RNAs relative to the WT were calculated using an unpaired, two-tailed t-test with Welch's correction for unequal variances, and the p-value for qRRM1,2^{W58A,Y155A} binding to 5′-AGGGA RNA relative to the WT was calculated using an unpaired, one-tailed t-test with Welch's correction.

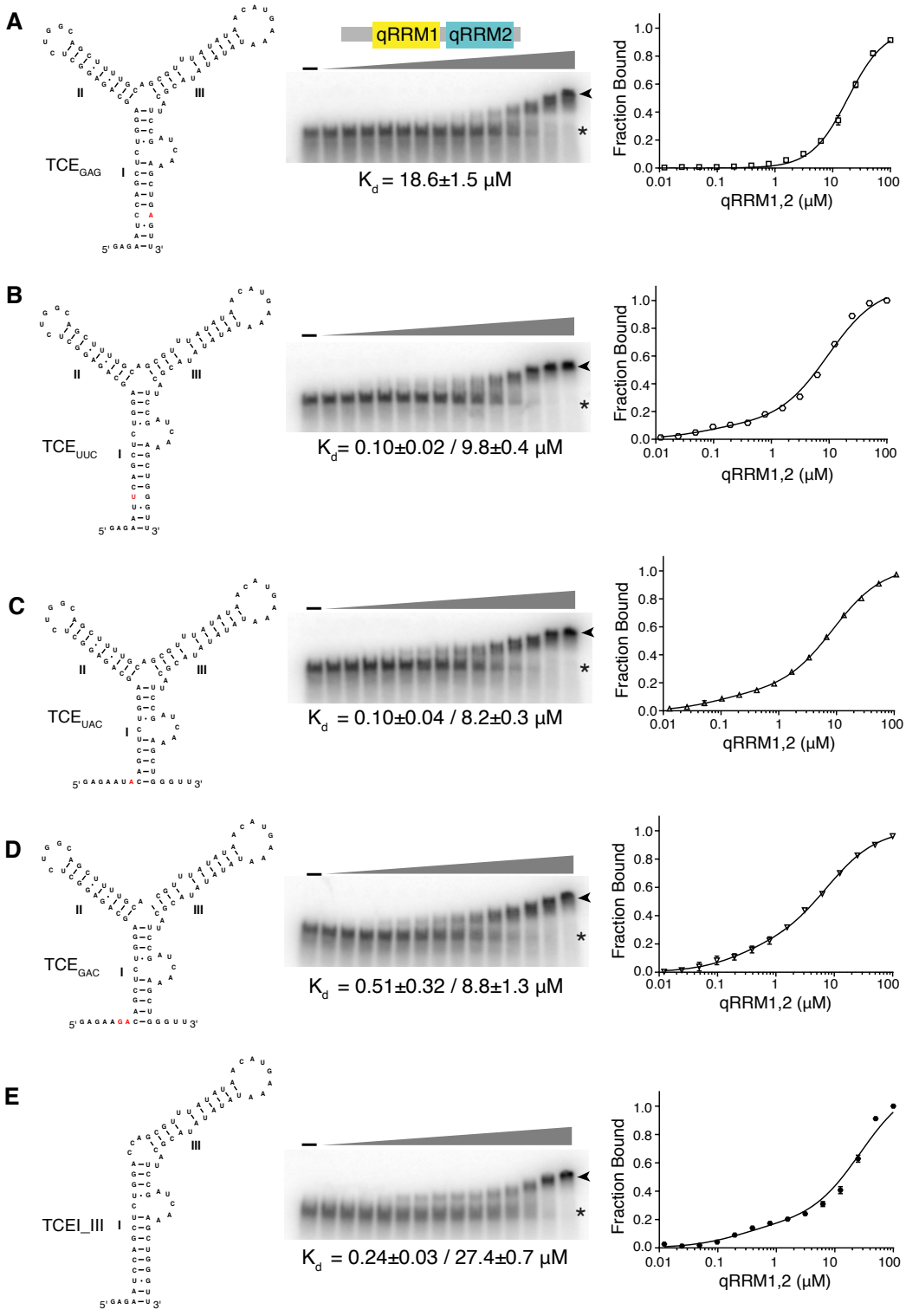

Figure S1. Effect of TCE mutations on Glo binding, related to Figure 3. (A-E) Predicted secondary structures of TCE_{GAG} (A), TCE_{UUC} (B), TCE_{UAC} (C), TCE_{GAC} (D), and TCEI_III (E) RNAs are shown at left. Middle panels show representative EMSAs of binding of Glo qRRM1,2 to the corresponding TCE mutant RNA, with data plotted at right. The highest protein concentration (right-most lanes) is 100 μM and 2-fold serial dilutions were assayed. No protein was added to the binding reactions in the lanes marked '-'. The positions of unbound RNA (asterisk) and Glo qRRM1,2:RNA complexes (arrowhead) RNA are indicated. Three technical replicates of EMSAs were performed, and apparent K_d values shown are mean ± SEM.

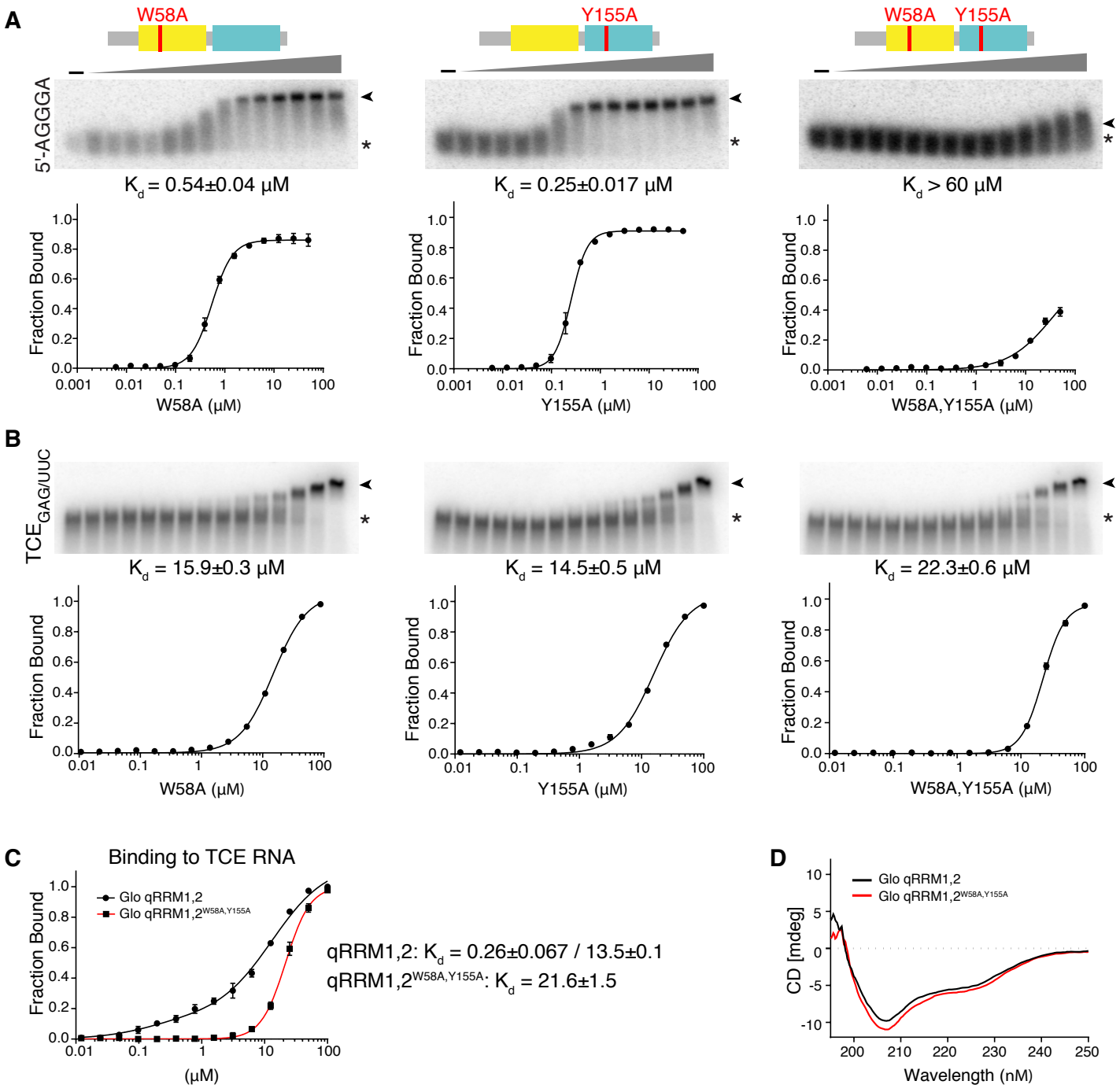

Figure S2. Mutation of loop residues selectively disrupts G-tract RNA binding, related to Figure 4. Representative EMSAs of binding of Glo qRRM1,2 mutants to 5′-AGGGA (A) or $TCE_{GAG/UUC}$ (B) RNAs with schematic representations of the mutants above and data plotted below. The highest protein concentrations (right-most lanes) are 100 μM for $TCE_{GAG/UUC}$ assays and 50 μM for 5′-AGGGA assays, and 2-fold serial dilutions were tested. No protein was added to the binding reactions in the lanes marked '-'. The positions of unbound RNA (asterisk) and Glo qRRM1,2:RNA complexes (arrowhead) RNA are indicated. Three technical replicates of EMSAs were performed, and apparent K_d values shown are mean ± SEM. (C) Higher affinity binding of Glo to the TCE is mediated by G-tract binding residues. Representative plots for binding of Glo qRRM1,2^{W58A,Y155A} (red) or wild-type Glo qRRM1,2 to TCE (black) are superimposed. (D) Circular dichroism spectra of Glo qRRM1,2 (black) and Glo qRRM1,2^{W58A,Y155A} (red) proteins.

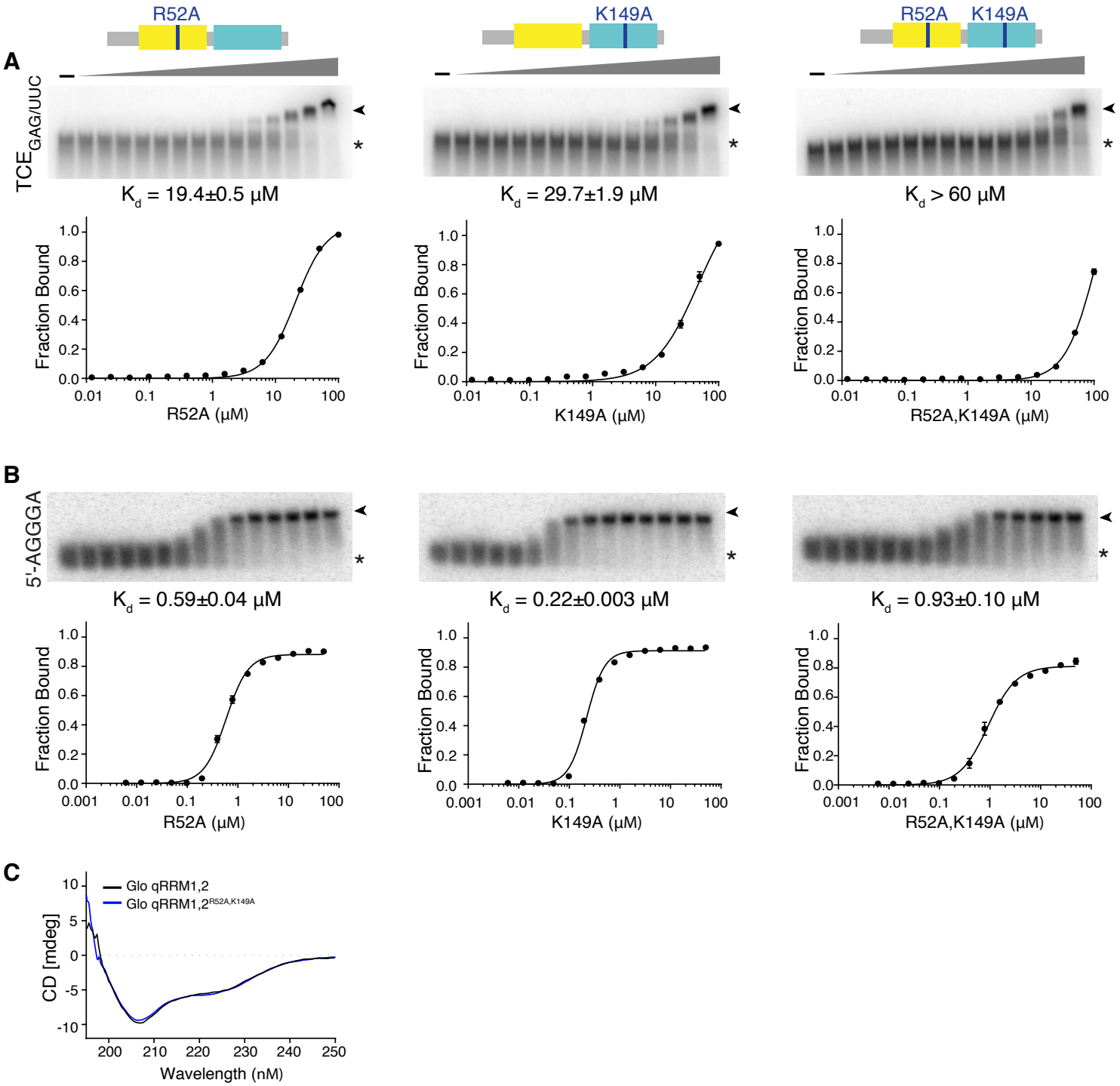

Figure S3. Mutation of basic RNP2 residues selectively disrupts TCEIII UA-rich motif binding. related to Figure 4. Representative EMSAs of binding of Glo qRRM1,2 mutants to TCE$_{GAG/UUC}$ (A) or 5′-AGGGA (B) RNAs with schematic representations of the mutants above and data plotted below. The highest protein concentrations (right-most lanes) are 100 μM for TCE$_{GAG/UUC}$ assays and 50 μM for 5′-AGGGA assays, and 2-fold serial dilutions were tested. No protein was added to the binding reactions in the lanes marked '-'. The positions of unbound RNA (asterisk) and Glo qRRM1,2:RNA complexes (arrowhead) RNA are indicated. Three technical replicates of EMSAs were performed, and apparent K_d values shown are mean ± SEM. (D) Circular dichroism spectra of wild-type Glo qRRM1,2 (black) and Glo qRRM1,2^{R52A,K149A} (blue) proteins.

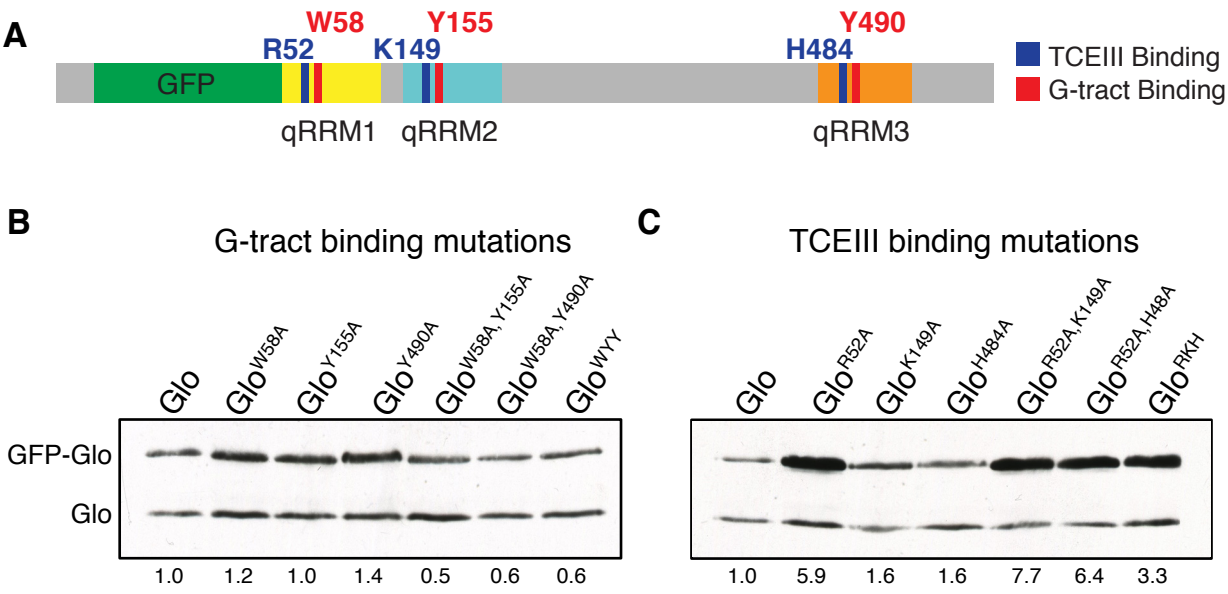

Figure S4. Expression of GFP-Glo transgenes, related to Figure 5. (A) Schematic representation of GFP-Glo protein, colored as in Figure 5, with a summary map of the alanine substitutions that were assayed for function *in vivo*. (B, C) Immunoblot analysis of Glo in extracts of ovaries from transgenic females expressing wild-type GFP-Glo or GFP-Glo proteins with either G-tract binding mutations (B) or TCEIII binding mutations (C). The blot was probed with anti-Glo antibody to detect both endogenous Glo and GFP-Glo. Relative abundance of GFP-Glo proteins, indicated below the blots, was quantified by normalization to endogenous Glo in the same sample and to wild-type GFP-Glo.

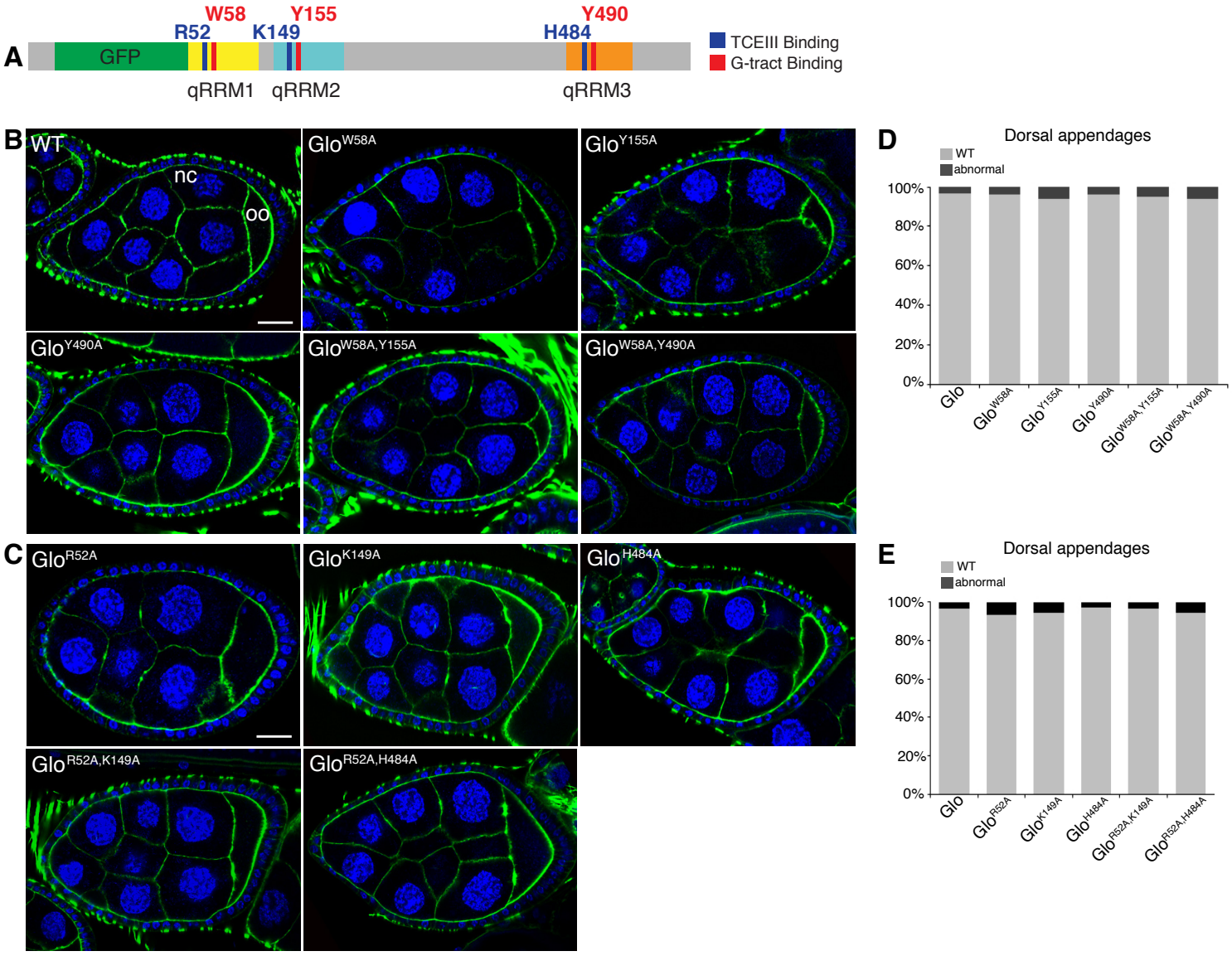

Figure S5. The Glo G-tract binding mode is required for Glo function in nurse cell chromosome disperson, related to Figure 7. (A) Schematic representation of GFP-Glo protein, colored as in Figure 5, with a summary map of the alanine substitutions that were assayed for function *in vivo*. (B,C) Confocal images of *glo* mutant egg chambers expressing GFP-Glo with either G-tract binding (B) or TCEIII binding (C) mutations. Nuclei were stained with DAPI (blue) and the actin cytoskeleton was stained with phalloidin (green). The nurse cells (nc) and oocyte (oo) are indicated. Scale bar=10 µm. (D, E) Quantification of the percentage of eggs from G-tract binding mutants (B) or TCEIII binding mutants (D) with dorsal appendage defects, including shortened, laterally expanded, fused, and/or missing appendages.

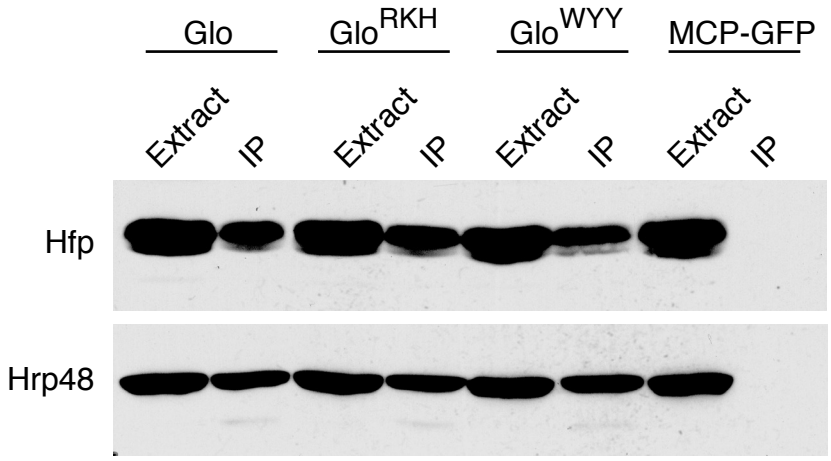

Figure S6. Glo mutant proteins interact with Hfp and Hrp48, related to Figure 7. Anti-GFP immunoprecipitation of extracts from ovaries expressing either wild-type GFP-Glo or the GFP-Glo G-tract binding triple mutant (Glo^{WYY}) or the GFP-Glo TCEIII binding triple mutant (Glo^{RKH}). Total extract and immunoprecipitates were analyzed by immunoblotting with antibodies to Hfp and Hrp48. Ovaries expressing an unrelated RNA-binding protein, MCP-GFP, were used as a negative control.

SUPPLEMENTAL EXPERIMENTAL PROCEDURES

Protein Expression and Purification

The cDNA sequences encoding the qRRM domains of Glo (qRRM1; 45-141, qRRM2; 142-234, qRRM3; 475-562, and qRRM1,2; 1-244) were subcloned into pET15b (Novagen), which encodes an N-terminal His_6-tag. Individual qRRM domains were expressed in *E. coli* strain BL21-CodonPlus (DE3)-RIL (Agilent Technologies) at 20 °C overnight after induction with 0.5 mM IPTG. The cells were collected by centrifugation, and pellets were resuspended in lysis buffer (50 mM Tris-HCl pH 8.0, 500 mM NaCl) and stored at −80 °C until use. The cells were disrupted by sonication and the soluble fraction was applied to a Ni-NTA agarose column (Thermo Scientific). After thorough washing with lysis buffer containing 20 mM imidazole, protein was eluted with lysis buffer containing 400 mM imidazole. For crystallization, the His_6 tag was cleaved overnight with 5 U of thrombin (Novagen). Glo qRRM proteins were further purified using a HiLoad 16/60 Superdex 75 column (GE Healthcare) equilibrated with lysis buffer, and peak fractions were pooled. For Glo qRRM1 purification, the pooled fractions were dialyzed against a buffer containing 50 mM Tris-HCl, pH 8.0, 20 mM NaCl and purified further using a HiTrap Heparin column (GE Healthcare). Bound protein was eluted using a 0-1 M NaCl linear gradient in 50 mM Tris-HCl, pH 8.0. Peak fractions were pooled and dialyzed against a buffer containing 20 mM Tris-HCl, pH 8.0, 100 mM NaCl and then concentrated to 10 mg/ml. For Glo qRRM2 purification, the pooled fractions were dialyzed against a buffer containing 50 mM Tris-HCl, pH 8.0, 100 mM NaCl and purified further using a HiTrap Heparin column (GE Healthcare). Bound protein was eluted using a 0.1-1 M NaCl linear gradient in 50 mM Tris-HCl, pH 8.0. Peak fractions were pooled and dialyzed against a buffer containing 20 mM Tris-HCl,

pH 8.0, 500 mM NaCl and then concentrated to 9 mg/ml. For Glo qRRM3 purification, pooled fractions were dialyzed against a buffer containing 50 mM Tris-HCl, pH 8.0, 100 mM NaCl. The dialyzed sample was applied to HiTrap Heparin column, HiTrap Q column (GE Healthcare), and HiTrap SP column (GE Healthcare) sequentially to remove contaminating proteins that bound to these columns. Unbound fractions containing Glo qRRM3 protein were pooled and dialyzed against a buffer containing 20 mM Tris-HCl, pH 8.0, 100 mM NaCl, then concentrated to 10 mg/ml.

Individual Glo qRRM domains for *in vitro* binding assays were purified by Ni-NTA agarose chromatography as described above, followed by purification on a HiLoad 16/60 Superdex 75 column (GE Healthcare) equilibrated with lysis buffer. The peak fractions were pooled and dialyzed against a buffer containing 20 mM HEPES-NaOH pH 7.9, 200 mM NaCl, and then concentrated.

Wild-type Glo qRRM1,2 protein and qRRM1,2 mutants generated by site-directed mutagenesis (Agilent Technologies) were purified by the same procedure as individual Glo qRRM proteins for *in vitro* binding assays. Following purification on a HiLoad 16/60 Superdex 75 column (GE Healthcare), peak fractions were pooled and dialyzed against a buffer containing 50 mM Tris-HCl pH 8.0, 50 mM NaCl, then purified further using a HiTrap Heparin column (GE Healthcare). Bound proteins were eluted using a 0.05-1 M NaCl linear gradient in 50 mM Tris-HCl, pH 8.0. Peak fractions were pooled and dialyzed against a buffer containing 20 mM HEPES-NaOH, pH 7.9, 200 mM NaCl, and then concentrated. To confirm correct folding of the mutant proteins, we assessed protein folding by circular dichroism (CD) and found no differences in the spectra of wild-type Glo qRRM1,2, Glo qRRM1,2^{W58A,Y155A}, and Glo qRRM1,2^{R52A,K149A} proteins (Figure S2, Figure S3). The CD spectra were measured on a JASCO

J-810 CD spectrometer at room temperature. For each sample (200 µl in a 0.1 cm light-path cell), four scans were accumulated in the wavelength range of 190–260 nm with a 0.2 nm step size. Protein samples were 100 µg/ml in 20 mM Na phosphate, pH 8.0, 100 mM NaCl. The raw CD data were adjusted by subtracting a buffer blank. CD spectra of wild-type and mutant proteins displayed negative ellipticities at 208/222 nm and 215 nm, which indicate the presence of α helices and β strands, respectively.

Crystallization, Data Collection, Structure Determination and Refinement

Crystals of Glo qRRM1 were prepared by the sitting-drop vapor diffusion method at 4 °C. Sitting drops contained 250 nl of protein mixed with 250 nl of reservoir solution (0.2 M ammonium sulfate, 0.1 M Na acetate pH 4.6, 30% w/v PEGMME 2000). Crystals of Glo qRRM2 or qRRM3 were prepared by the hanging-drop vapor diffusion method at 20 °C. Hanging drops contained 1 µl of protein mixed with 1 µl of reservoir solution (qRRM2: 0.2 M ammonium acetate, 20% v/v PEG 3350; qRRM3: 0.5 M ammonium sulfate, 0.1 M Na cacodylate pH 6.4, 1.0 M lithium sulfate). Prior to data collection, crystals were transferred to a cryoprotectant solution containing 15% glycerol and flash cooled to -180 °C. X-ray diffraction data for crystals of qRRM1 and qRRM3 were collected using a conventional X-ray source (Rigaku 007HF rotating anode equipped with VariMax HF mirrors and a Saturn 944 CCD detector) and for crystals of qRRM2 were collected at the SER-CAT Beamline 22-ID at the Advanced Photon Source, Argonne National Laboratories. Diffraction data were processed using the program package HKL2000 (HKL Research Inc. (Otwinowski and Minor, 1997). The resolution limits of data collection for qRRM1, qRRM2 and qRRM3 were restricted to 1.54, 1.55 and 1.99 Å, respectively, due to the detector settings during data collection, although the crystals

might diffract to higher resolution. The structures were determined by molecular replacement using the program Molrep (Vagin and Teplyakov, 2000). The NMR structures of qRRM1, qRRM2 and qRRM3 of human hnRNP F were used as the search models for Glo qRRM1, qRRM2 and qRRM3, respectively. Model building was carried out with the program Coot (Emsley and Cowtan, 2004). The programs Refmac5 (Murshudov et al., 1997) and Phenix.refine (Adams et al., 2010) were used for refinement. The structures displayed good geometry when analyzed by MolProbity (Chen et al., 2010).

In vitro Transcription

TCE and TCE mutant RNAs were produced by *in vitro* transcription. DNA templates were amplified by PCR using a 5' primer containing the T7 promoter sequence with a GAG sequence that replaces the GCG at the 5′ end of the TCE (Gavis et al., 1996) to stimulate *in vitro* transcription by T7. Thus all transcripts begin with GAG (see Figure 3). TCE mutations were encoded in the corresponding templates. The PCR products were used directly as templates for *in vitro* transcription. *In vitro* transcription with T7 RNA polymerase was performed in a buffer containing 40 mM Tris-HCl, pH 8.0, 2.5 mM spermidine, 26 mM $MgCl_2$, 0.01% v/v Triton X-100, 1 mM DTT, 4 mM NTPs, 16 mM GMP, 40 U RNase inhibitor, and 0.5 U pyrophosphatase. Reactions were incubated for 4 hr at 37 °C. Reactions were then supplemented with 50 U of DNase I and 10x DNase reaction buffer (400 mM Tris-HCl, pH 7.9, 100 mM NaCl, 60 mM $MgCl_2$, 10 mM $CaCl_2$) and incubated for 30 min at 37 °C. RNA products were purified by phenol/chloroform extraction followed by ethanol precipitation. RNA was further purified by electrophoresis on a 10% polyacrylamide-urea gel (Invitrogen) in 1x TBE buffer. Target bands were detected by UV shadowing, excised from the gel, and incubated in RNA elution buffer (20

mM Tris-HCl, pH 7.5, 250 mM Na acetate, 1 mM EDTA, 0.25% w/v SDS) overnight at room temperature. Eluted RNA was diluted to 10 ml and purified further using a HiTrap Q column (GE Healthcare). Bound RNAs were eluted using a 0.05-1 M NaCl linear gradient in 50 mM Tris-HCl, pH 8.0. Peak fractions containing target RNAs were pooled, ethanol precipitated, and resuspended in DEPC-treated water.

Electrophoretic Mobility Shift Assay

TCE and TCE mutant RNAs were produced by *in vitro* transcription as described above, and a 5′-AGGGA RNA oligonucleotide was generated by RNA synthesis (GE Dharmacon). RNAs were radiolabeled at the 5′ end using [γ-^{32}P] ATP and T4 polynucleotide kinase, then purified using an Illustra MicroSpin G-25 column (GE Healthcare). TCE and TCE mutant RNAs were prepared by heating to 90 ºC for 5 min, and then slowly cooling to room temperature. The 5′-AGGGA RNA oligonucleotide was incubated at 90 °C for 5 min in 50 mM Tris, pH 8.0 and then cooled on ice. This procedure yielded single-stranded RNA that bound to qRRMs as analyzed by size exclusion chromatography. RNA-binding reactions included 0.9 nM radiolabeled RNA and increasing concentrations (2-fold) of protein in a binding buffer containing 20 mM HEPES, pH 7.9, 50 mM NaCl, 50 mM KCl, 2 mM $MgCl_2$, 0.02% v/v Tween-20, 1 μg/ml yeast tRNA, 0.1 mg/ml poly(rU), and 5% v/v glycerol. Binding reactions were incubated for 1 hr at room temperature and immediately separated by electrophoresis on 10% polyacrylamide gels (Invitrogen) in 1x TBE buffer at 100 V for 30 min at 4 °C. Gels were dried and exposed to storage phosphor screens for 6–20 hr, scanned with a Typhoon 8600 Imager, and the band intensities were quantified with ImageQuant 5.2. The data were analyzed and K_d values were calculated via non-linear regression analysis for one- or two-site binding with GraphPad Prism 6.

Three technical replicates of all binding assays were performed, and K_d values are reported as mean ± standard error of the mean (SEM).

We assessed the stoichiometry of Glo qRRM1,2 protein binding to RNA by EMSA using 100 µM 5′-AGGGA or 500 µM TCE RNA and protein-RNA ratios of 0.1, 0.25, 0.5, 0.75, 1.0, 1.5 and 2.0. Glo qRRM1,2 binding to 5′-AGGGA RNA saturated at a protein-RNA ratio of ~0.5, corresponding to two 5′-AGGGA molecules per Glo qRRM1,2. Glo qRRM1,2 binding to TCE RNA was more complex and saturated at a protein-RNA ratio of ~1.5, which is not conclusive. Interpretation of the stoichiometry EMSA is complicated due to the two-site binding model, but the 1.5 protein-RNA ratio may correspond to a mixture of 1:1 and 2:1 protein-RNA complexes. Since full-length Glo contains three qRRM domains, the 2:1 complexes might include the binding of a third qRRM domain from a second protein.

Immunoprecipitation

Ovaries from well-fed females were dissected in PBS and homogenized in IP buffer [10 mM Tris-HCl pH 7.5, 150 mM NaCl, 0.5 mM EDTA, 0.5% NP-40, 0.1mM PMSF, 1x complete protease inhibitor cocktail (Roche)]. Extracts were subsequently cleared by centrifugation at 13,000 rpm for 10 min at 4° C and supplemented with 100 µg/ml RNase A and 100 units/ml RNase One (Promega). Cleared extracts were then incubated with GFP_TRAP®_M beads (ChromoTek) for 2 hours at 4° C. Eluted protein complexes were resolved by SDS-PAGE, transferred to nitrocellulose membrane and detected by immunoblotting and chemiluminescence. Primary antibody concentrations: 1:20 mouse anti-Hfp (6G10; *Drosophila* Studies Hybridoma Bank); 1:5000 rabbit anti-Hrp48 (Siebel et al., 1994).

REFERENCES

Adams, P.D., Afonine, P.V., Bunkoczi, G., Chen, V.B., Davis, I.W., Echols, N., Headd, J.J., Hung, L.W., Kapral, G.J., Grosse-Kunstleve, R.W.*, et al.* (2010). PHENIX: a comprehensive Python-based system for macromolecular structure solution. Acta. Crystallogr. D. Biol. Crystallogr. *66*, 213-221.

Chen, V.B., Arendall, W.B., 3rd, Headd, J.J., Keedy, D.A., Immormino, R.M., Kapral, G.J., Murray, L.W., Richardson, J.S., and Richardson, D.C. (2010). MolProbity: all-atom structure validation for macromolecular crystallography. Acta. Crystallogr. D. Biol. Crystallogr. *66*, 12-21.

Emsley, P., and Cowtan, K. (2004). Coot: model-building tools for molecular graphics. Acta. Crystallogr. D. Biol. Crystallogr. *60*, 2126-2132.

Gavis, E.R., Lunsford, L., Bergsten, S.E., and Lehmann, R. (1996). A conserved 90 nucleotide element mediates translational repression of *nanos* RNA. Development *122*, 2791-2800.
Murshudov, G.N., Vagin, A.A., and Dodson, E.J. (1997). Refinement of macromolecular structures by the maximum-likelihood method. Acta. Crystallogr. D. Biol. Crystallogr. *53*, 240-255.

Otwinowski, Z., and Minor, W. (1997). Processing of X-ray diffraction data collected in oscillation mode. Method Enzymol *276*, 307-326.
Vagin, A., and Teplyakov, A. (2000). An approach to multi-copy search in molecular replacement. Acta. Crystallogr. D. Biol. Crystallogr. *56*, 1622-1624.

Siebel, C.W., Kanaar, R., Rio, D.C. (1994). Regulation of tissue-specific P-element pre-mRNA splicing requires the RNA-binding protein PSI. Genes Dev. *8*, 1713–1725.